AD-A049 505 NAVAL RESEARCH LAB WASHINGTON D C F/G 20/9
A THEORY OF ELECTRON ENERGY CONFINEMENT IN TOKAMAKS.(U)
OCT 77 W M MANHEIMER, T ANTONSEN ES-77-A-01-6021
UNCLASSIFIED NRL-MR-3551 SBIE-AD-E000 093 NL

1 OF 1
AD
A049505

END
DATE
FILMED
3-78
DDC

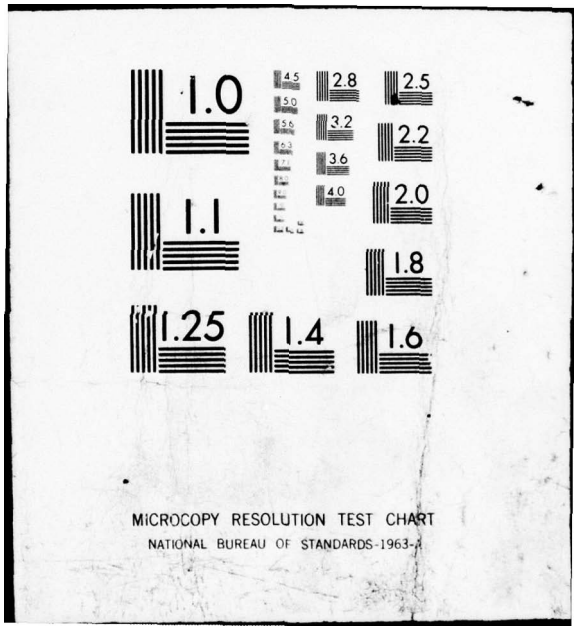
1.0
1.1
1.25
1.4
1.6
1.8
2.0
2.2
2.5
2.8
3.2
3.6
4.0
4.5
5.0
5.6
MICROCOPY RESOLUTION TEST CHART
NATIONAL BUREAU OF STANDARDS-1963-A

NRL Memorandum Report 3551

A Theory of Electron Energy Confinement in Tokamaks

W. M. MANHEIMER and T. M. ANTONSEN, JR.

Plasma Physics Division

October 1977

NAVAL RESEARCH LABORATORY
Washington, D.C.

SECURITY CLASSIFICATION OF THIS PAGE (When Data Entered)

REPORT DOCUMENTATION PAGE

READ INSTRUCTIONS BEFORE COMPLETING FORM

1. REPORT NUMBER: NRL Memorandum Report 3551
2. GOVT ACCESSION NO.
3. RECIPIENT'S CATALOG NUMBER

4. TITLE (and Subtitle): A THEORY OF ELECTRON ENERGY CONFINEMENT IN TOKAMAKS,
5. TYPE OF REPORT & PERIOD COVERED: Interim report on a Continuing NRL Problem
6. PERFORMING ORG. REPORT NUMBER

7. AUTHOR(s): W.M. Manheimer and Thomas Antonsen, Jr.
8. CONTRACT OR GRANT NUMBER(s): NRL-MR-3551

9. PERFORMING ORGANIZATION NAME AND ADDRESS: Naval Research Laboratory, Washington, D.C. 20375
10. PROGRAM ELEMENT, PROJECT, TASK AREA & WORK UNIT NUMBERS: NRL Problem No. HO2-58; ES-77-A-01-6021

11. CONTROLLING OFFICE NAME AND ADDRESS: Energy Research and Development Administration, Germantown, Md. 20545
12. REPORT DATE: October 1977
13. NUMBER OF PAGES: 29

14. MONITORING AGENCY NAME & ADDRESS (if different from Controlling Office)
15. SECURITY CLASS. (of this report): UNCLASSIFIED
15a. DECLASSIFICATION/DOWNGRADING SCHEDULE

16. DISTRIBUTION STATEMENT (of this Report)

Approved for public release; distribution unlimited.

18. SBIE
19. AD-E000 093

DDC RECEIVED FEB 6 1978 B

17. DISTRIBUTION STATEMENT (of the abstract entered in Block 20, if different from Report)

18. SUPPLEMENTARY NOTES

19. KEY WORDS (Continue on reverse side if necessary and identify by block number)

drift wave turbulence
marginal stability
electron energy confinement time

20. ABSTRACT (Continue on reverse side if necessary and identify by block number)

(U) A one dimensional thermal transport code has been employed to study electron energy confinement in tokamaks. At each time step of the computations each point in the profile is examined to determine whether it is linearly stable to either the dissipative trapped electron mode or the internal kink and tearing modes. If the point is determined to be unstable an anomalously large electron thermal conductivity is turned on in the vicinity of that point. The electron temperature profile is found to relax to a marginally stable state. Our code predicts the scaling of confinement time with density in Alcator, and the scaling of temperature half-width with q(a) in TFR.

DD FORM 1 JAN 73 1473 EDITION OF 1 NOV 65 IS OBSOLETE S/N 0102-LF-014-6601

SECURITY CLASSIFICATION OF THIS PAGE (When Data Entered)

251 950

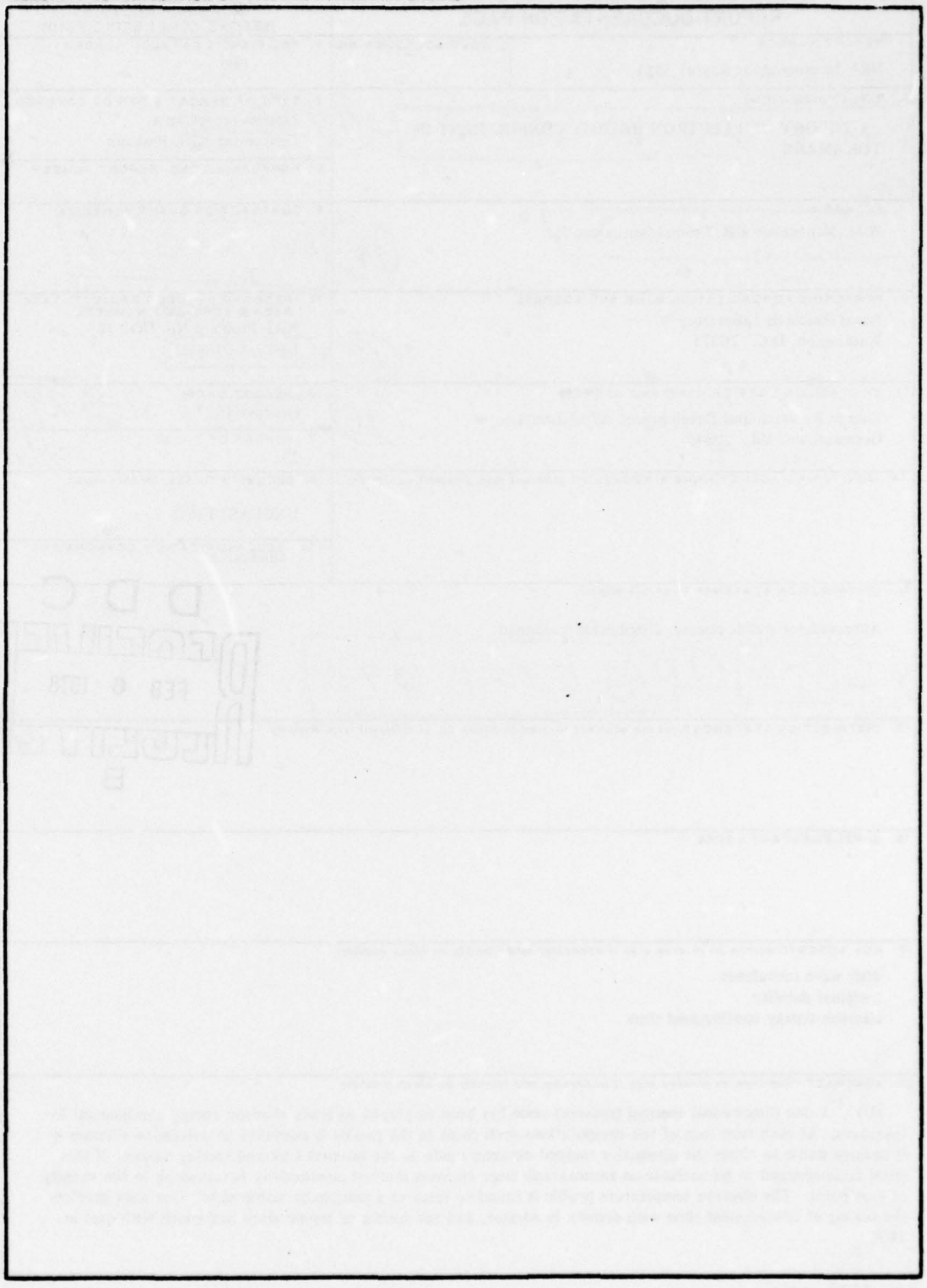

CONTENTS

A THEORY OF ELECTRON ENERGY CONFINEMENT IN TOKAMAKS

I. Introduction

The problem of electron energy flux is one of the most perplexing problems in tokamak research. The most recent transport codes, have focussed on the six regime transport model [1]. There, depending on the parameters, the plasma is subject to one of a number of instabilities. The nonlinear theory of each instability then gives rise to a transport coefficient in the appropriate regime. Other codes have focussed on the so called pseudo classical model for transport [2-7].

This paper examines another approach to the problem of anomalous transport in tokamaks, the so called marginal stability approach [8,9]. The idea is that as soon as the plasma becomes unstable, the electron transport coefficient jumps abruptly to a large value. The resulting enhanced transport forces the plasma to a stable regime. If some other mechanism forces the plasma towards instability, the logical steady state is at the marginally stable point. The basic idea behind the marginal stability approach is described in Ref. 8. Recently, we have derived relative temperature profiles for tokamaks [9]. This paper is an extension of our earlier work. The marginal stability approach has also worked well in describing the behavior of resistive shocks [10], the behavior of plasma in electric fields [8,11], screw pinches [12], and also the behavior of trapped particles in the magnetosphere [13]. Also, there is apparantly some thermodynamic evidence for the occurence of a marginally stable state [14]. There are at least two recent experimental results, the qualitative features of which are explained very naturally be marginal stability theory. The first is the result of heating TFR with neutural beams [15]. Although a large amount of beam power was deposited into the electrons the electon temperature did not change at all in one experiment, and changed only very slightly (less than 10%) in another. This result is certainly consistent with the idea that the electron temperature profile is resting at some marginally stable value. The harder it is pushed into the unstable regime, the harder the plasma fights back. The result is that the temperature profile always sits near the marginally stable profile no matter how hard is it pushed.

The second is the results of heat pulse propagation studies in ORMAK [16]. A pulse of energy is dumped from the center of the plasma $r/a \equiv 0$ (a = limiter radius) to about $r/a \equiv .25$. The propagation of the heat pulse to $r/a \equiv .75$ is studied by X-rays. The remarkable fact is that the time for pulse propagation outward is considerably shorter than the energy containment time. This is so even though the relative temperature perturbation is quite small. This too is consistent with the plasma temperature remaining at a marginally stable profile; any increase in temperature drives the plasma to an unstable state, and is therefore rapidly expelled.

To examine whether the concept of marginal stability is viable for a tokamak plasma, we have put together a small transport code which solves for electron and ion temperatures. A large electron thermal conductivity is turned on whenever the plasma becomes linearly unstable. Our basic assumption is that in a real Tokamak the anaomalous electron thermal conductivity that would result if the plasma were forced into an unstable state is large enough to maintain the temperature near a linearly marginaly stable profile. Thus, as far as determining

Manuscript submitted June 29, 1977.

the profile is concerned all that is necessary to know is the marginal stability condition (the conditions under which the transport should become large). The magnitude of the transport in an unstable plasma affects only the rate at which the plasma is driven to the marginally stable state.

Our approach is similar to a quasilinear theory of transport with the additional assumption that the characteristic time over which the instability can develop and field amplitudes vary is short compared to the time scale of the gross energy confinement in the plasma. Thus if the field amplitudes are quasisteady indicating saturation of the instability the linear growth rate must be nearly zero. This code however does not model as many physical effects as does others[1]. Specifically we do not solve for the density profile, the impurity transport or the neutural transport. Also, we assume that the current is always its steady state value ($J = \sigma(T_e)E$), so that the code does not solve for skin effect either. Our goal is only to see whether the marginal stability approach is a viable concept. If it is, a more complete code can be extended or modified to incorporate it.

In order to utilize this approach, it is necessary to carefully examine the stable and unstable regimes of parameter space. We find that the instability does not depend only on collisionality. The density gradient, temperature gradient and shear all play important roles. One particularly important effect is that the temperature gradient can be strongly stabilizing at low enough temperatures, so that the outer region of the plasma is generally classical. At higher temperatures only the shear is stabilizing, and the electron temperature picks out the profile at which shear stabilization just balances the temperature and density gradient induced growth rates.

The results of our code are sufficiently encouraging that we conclude that the marginal stability approach is viable. Its theoretical foundation is very simple and understandable; it does not rely at all on complex, speculative nonlinear theories of many different instabilities. The only uncertainties involved are those inherent in linear theory.

As far as confinement times are concerned, our predictions are generally too high by a factor of from two to five. However temperature profiles and scaling laws show much better agreement with experiment. Two scaling laws which our code predicts are the increase of confinement time with density in Alcator, and the fact that the temperature half width and the radius of the $q = 1$ surface depend only on a single parameter, $q(a)$, as measured in TFR. Furthermore, our calculations of fluctuation levels also agree resonably with those measured in ATC.

II. The Code

A – Basic Fluid Code

In order to test whether marginal stability is a reasonable approach to the problem of anomalous electron energy transport in tokamaks, we have constructed a simple computer code[17]. The equations which are solved numerically are

$$\frac{3}{2} n \frac{\partial T_e}{\partial t} = \frac{1}{r} \frac{\partial}{\partial r} r(K_{ce} + K_{an}) \frac{\partial T_e}{\partial r} + E \cdot J - 3\nu_e \frac{m}{M} n (T_e - T_i) \qquad (1a)$$

$$\frac{3}{2} n \frac{\partial T_i}{\partial t} = \frac{1}{r} \frac{\partial}{\partial r} r K_{ci} \frac{\partial T_i}{\partial r} + 3\nu_e \frac{m}{M} n (T_e - T_i) \qquad (1) \qquad (1b)$$

$$E = J/\sigma \tag{1c}$$

where $T_{e(i)}$ are the electron (ion temperature), J is the current density, E is the toroidal electric field, assumed to be independent of radius, σ is the electrical conductivity given by Rutherford [1],

$$\sigma = \frac{n_e e^2}{m} \tau_e \left(\frac{0.457 Z_{ef}}{1.077 + Z_{ef}} + 0.29 Z_{ef} \right)^{-1}, \tag{2}$$

τ_e is the electron ion momentum exchange collision time

$$\nu_e = \tau_e^{-1} = \frac{4\sqrt{2\pi} n e^4 \ln \Lambda}{3 m^{1/2} T_e^{3/2}} \tag{3}$$

where Z_{ef} is the effective charge of the plasma. Also, K_{ce} and K_{ci} are the neoclassical expression for electron and ion thermal conductivity. Here was adopt the expression given by Rutherford, Duchs [1,2],

$$K_{ce} = \frac{1.81}{1 + 0.36\nu_e^*} \frac{Z_{ef} n \rho_{e\theta}^2}{\tau_e} \left(\frac{r}{R} \right)^{1/2} + \frac{Z_{ef} \rho_e^2 n}{\tau_e} \left(1 + 1.6 \frac{r^2 B^2}{R^2 B_\theta^2} \right)$$

$$K_{ci} = \frac{0.68}{1 + 0.36\nu_i^*} \frac{Z_{ef} n \rho_{i\theta}^2}{\tau_i} \left(\frac{r}{R} \right)^{1/2} + \frac{Z_{ef} \rho_i^2 n}{\tau_i} \left(1 + 1.6 \frac{r^2 B^2}{R^2 B_\theta^2} \right). \tag{4}$$

Above, $\rho_{e\theta}$ ($\rho_{i\theta}$) is the electron (ion) larmor radius in the poloidal field, τ_i is the ion-ion collision time

$$\tau_i = (3 m_i^{1/2} T_i^{3/2}) (4\sqrt{\pi} n e^4 \ln \Lambda_i)^{-1}. \tag{5}$$

The quantities ν_i^* and ν_e^* are the ratio of effective ion or electron collision frequency $(\tau\epsilon)^{-1}$ to the ion or electron bounce frequency

$$\nu_e^* = \frac{1}{2}(1 + Z_{ef}) R^{3/2} B/\tau_e r^{1/2} B_\theta (T_e/m)^{1/2} \tag{6a}$$

$$\nu_i^* = Z_{ef} R^{3/2} B/\tau_i r^{1/2} B_\theta (T_i/M)^{1/2}, \tag{6b}$$

and all other notation is standard. Notice that the fluid equations solved have no magnetic diffusion, but rather assume the steady state value for current. Thus, the code does not correctly predict the approach to equilibrium. However it should predict the correct steady state. Finally, K_{an} is the anomalous electron thermal conductivity. Consistent with our assumption of marginal stability, we take for K_{an}, a function which rises very suddenly at the onset of instability.

There are two instabilities we consider here. The first are internal kink [18,19] and tearing modes which occur at the center of the plasma. These are observed to have an $m = n = 1$ structure and are detected by saw-tooth oscillations on the soft X-ray signals [20,21]. To simulate the effect of these modes we assume K_{an} jumps to a large value whenever the safety factor $q = rB/RB_\theta$ is less than unity. This is roughly the same approach taken in the Princeton numerical simulations [1].

The second instability, which we concentrate on here is the dissipative trapped electron mode [22]. This will be discussed more fully in a later subsection. For our purpose now, we can regard the plasma as unstable to this instability if the ratio of density gradient scale length to shear scale length, Θ, is less than some critical value Θ_{cr}. The form for the anomalous thermal conduction which we choose is

$$K_{an} = nD_B\left\{\frac{q^{-n'}}{1+q^{-n'}} + \frac{(\Theta/\Theta_{cr})^{-n}}{1+(\Theta/\Theta_{cr})^{-n}}\right\} \tag{7}$$

where D_B is the Bohm diffusion coefficient

$$D_B = \frac{cT}{16eB}, \tag{8}$$

and $n, n' >> 1$. We have called the functions in the parentheses thermostat functions because they jump sharply from zero to one as q and Θ/Θ_{cr} go from slightly greater than one to slightly less than one.

Many of the quantities in Eqs. (1) – (8) depend on density. Therefore to run the code, it is necessary to specify a density profile. In a later subsection, we discuss how the code could be extended to solve for the density profiles self consistently. For all of the work presented here however, density profiles are specified arbitrarially.

The remaining things to specify are boundary conditions for temperature and current. We choose an electron and ion temperature of 10 ev, at the limiter and consider the total current to be specified. This is equivalent to choosing a particular value of q at the limiter.

B – The Role of Nonlinear Theory

It is worth reiterating here that there is a very fundamental difference in the approach taken here and the approach taken by others. Generally plasma is assumed to exist in a linearly unstable state. The transport coefficient is determined by the fluctuation level which is limited by some local nonlinear effect, for instance resonance broadening[23], mode coupling[24,25], etc. Therefore, to get transport coefficients, it is essential to have a nonlinear theory of all relevant instabilities. In our approach, we assume the most effective stabilization mechanism is the relaxation of the plasma to a linearly stable state. If some mechanism forces the plasma towards instability, it is reasonable to assume that the plasma sits at marginal stability. For an Ohmically heated tokamak, this mechanism is the channeling of the current into the hotter regions in the center. This then increases the electron temperature gradient (since $T_e(r = a)$ is held fixed at 10ev)). However a steep electron temperature gradient drives trapped particle instabilities which then causes anomalous thermal conduction. Thus a dynamic balance should be possible, with the tokamak temperature profile sitting at marginal stability.

Needless to say, nonlinear theory of the relevant instabilities, plays a much less important role in this type of plasma, than it does if the plasma is assumed to be everywhere linearly unstable. This is not to say that nonlinear theory plays no role at all. Indeed, the proper evaluation of the thermostat functions, defined in the last section, can only be made through nonlinear theory. It is interesting to note however that the most recent studies[26] of stabilization of drift waves and trapped particle instabilities by resonance broadening show no nonlinear saturation unless $\gamma/\omega < (k_{||} v_i/\omega)^2$. That is, no saturation unless the mode is only slightly above marginal stability.

C – The Instability

It remains to determine Θ_{cr}. This can be done by examining the dispersion relation for trapped electron instability[22,27–31]. The theory of this instability is continually being refined, and it would be difficult to write an expression for growth rate which would be universally ac-

cepted at this time. The disperion relation we use neglects the coupling between poloidal and radial structure so it does not properly treat the two dimensional mode structure[31]. However it probably does reasonably approximate all of the significant physical effects.

The dispersion relation we use is[32]

$$\epsilon = S(b)\{\tau + \zeta\,[1 - \eta_i b^2\, G(b)]\} - 1 - \tau + \int_{UT} d^3v \frac{\omega - \omega_{*e}}{\omega - v_{||}/(Rq)} f_m + \int_T d^3v \frac{\omega - \omega_{*e}}{\omega + i\nu_{ef} - \omega_d} - i\delta_{ii} - i\zeta\,\tau^{-1}\,\Theta\, S(b)\,\{[\tau + \zeta(1 - \eta_i)]\, G(b) + \eta_i\,\zeta\,[1 + (1 - 2b^2)\, G(b)]\}^{1/2}\{\tau + \zeta[1 + \eta_i - \eta_i b^2 G(b)]\}^{1/2} = 0. \tag{9}$$

In Eq. (9) above $\tau = T_e/T_i$, $\zeta = \omega_*/\omega$, $\nu_{ef} = v_e^3/(v^3\tau_e\epsilon)$, $\omega_d = \omega_{*}\epsilon_n\, v^2/v_e^2$, $\epsilon = r/R$, $S(b) = I_o(b)e^{-b}$, $b = k^2\rho_i^2$, η_i is the density gradient scale length divided by the ion temperature gradient scale length, $G(b) = 1 - I_1(b^2)/I_o(b^2)$, UT denotes an integral over untrapped regions of electron velocity space ($v_{||}/v_{|} > \sqrt{2\epsilon}$ and also $\omega_b(v) > (\nu_e/\epsilon)(v_e/v)^3$ where $\omega_b(v) = \sqrt{2\epsilon}\, v/Rq$), and T denotes the integral over the trapped region of electron velocity space. The quantity $\omega_{*e} = \omega_*(1 + \eta_e\,(1/2\, mv^2/T_e - 3/2))$ where ω_* is the electron diamagnetic drift velocity and δ_{ii} is the ion collisional damping rate[33]

$$\delta_{ii} = .7\nu_{ii}\, b^4\left[\frac{T_e}{T_i} + \frac{\omega_*}{\omega}(1 - 0.1\,\eta_i)\right]/\omega \quad \text{for } k\rho_i < 1,$$

$$\text{and } \delta_{ii} = .9\nu_{ii}\, b\left[\frac{T_e}{T_i} + \frac{\omega_*}{\omega}(1 - 0.7\,\eta_i)\right]/\omega \quad \text{for } k\rho_i > 1. \tag{10}$$

To derive Eq. (9), we have split the electron velocity space up into trapped and untrapped regions. The $\omega_*\epsilon_n\,(v/v_e)^2$ term in the denominator of the trapped term is the effect of the drift resonances. Here $\epsilon_n = L_n/R$. In the untrapped term, we have assumed $k_{||} = 1/Rq$. To calculate the effect of shear induced damping, we have neglected the poloidal mode structure and have performed a Pearlstein-Berk[34] calculation of the shear damping assuming $k_r\rho_i << 1$ and also assuming that a mode unstable on one mode rational surface does not couple to waves on other rational surfaces. Unfortunately, this approximation is not valid for $k_\theta\rho_i$ larger than about 0.2. For larger $k\rho_i$, the calculation of shear induced damping is extremely complicated, involving the full two dimensional nature of the mode structure[31]. Preliminary indications are that shear is somewhat less effective a stabilization mechanism[31,35,36] than is described in Eq. (9). We have arbitrarily reduced the effect of shear stabilization in our code in certain circumstances by multiplying the last term in Eq. (9) by a factor less than unity in order to assess the consequences of this possibility.

We will now discuss qualitatively the effects of various terms in the dispersion relation.

1) In both the T and UT terms, the effect of a density gradient is destabilizing.

2) Shear is stabilizing for all k and all temperature.

3) An electron temperature gradient is stabilizing in the UT term.

4) An electron temperature gradient is destabilizing in the T term.

5) Ion-ion collisions are always stabilizing and can be an important stabilizing effect at low enough temperature.

From these facts, some rough qualitative features of the instability can be discerned. As the plasma temperature is lowered, there are fewer and fewer trappped particles to drive instability. Therefore as the temperature is lowered, the electron temperature gradient will at some point change from a destabilizing to a stabilizing effect. Since temperature profiles in tokamaks are generally steeper than density profiles, we expect the outer, cooler regions of the tokamak to be stable. As a very rough rule of thumb, we find that the electron temperature gradient changes from a destabilizing to a stabilizing effect at approximately the transition from the plateau regime to the Pfirsch-Schliter regime.

The next problem is to analyize the dispersion relation to find the critical shear for stability. To make any progress, it is necessary to make a few approximations, principally to shrink down the dimensionality of the parameter space. We wish to determine from Eq. (9) the value of Θ, the shear, necessary to stabilize all modes, that is we require $Im\{\omega(k\rho_i)\} \leqslant 0$ for all $k\rho_i$. To accomplish this we calculate the value of Θ necessary to stabilize the mode for each particular $k\rho_i$, call it $\hat{\theta}(k\rho_i)$, and select Θ_{cr} to be the largest of these values. Thus, we view the real and imaginary parts of Eq. (9) as two equations determing the two unknowns $\omega_r(\omega = \omega_r + i\gamma, \gamma = 0)$ and $\hat{\theta}(k\rho_i)$.

The real part of Eq. (9) does not involve $\hat{\Theta}$ and hence may be solved to determine ω_r. Once ω_r is known for each $k\rho_i$ it is a simple matter to substitute $\omega_r(k\rho_i)$ in the imaginary part of Eq. (9) to determine $\hat{\Theta}(k\rho_i)$. Here we point out that ω_r is the real frequency for a marginally stable mode and not necessarily the real part of the frequency for a damped mode. In our computations we assumed that the nonadiabatic electron response was negligible insofar as determining ω_r. In this case the equation for ω_r is given by,

$$S(b)\{\tau + \zeta[1 - \eta_i b^2 G(b)]\} - 1 - \tau = 0, \tag{11}$$

where $\tau = T_e/T_i$ and $\zeta = \omega^*/\omega$. Equation (11) was further simplied by assuming $\tau = 1.5$, and $\eta_i = 1.0$. This allowed us to calculate ω/ω^* as a function of $k\rho_i$ from the outset and, hence, it was not necessary to solve Eq. (11) at each point in the profile or each time step.

The imaginary part of Eq. (9) can be written as follows,

$$\Theta\,\Sigma(b) = f_1(\nu_e^*, \epsilon_n, \epsilon, \zeta, q) + \eta_e f_2(\nu_e^*, \epsilon_n, \epsilon, \zeta, q) - \delta_{ii}, \tag{12}$$

where

$$\Sigma = \zeta\tau S(b)\{[\tau + \zeta(1 - \eta_i)]G(b) + \eta_i\zeta[1 - (1 - 2b^2)G(b)]^{1/2}\}\{\tau + \zeta[1 + \eta_i - \eta_i b^2 G(b)]\}^{1/2}, \tag{13}$$

and f_1 and f_2 are functions involving integrals over velocity space that result from the nonadiabatic electron response.

The first term in Eq. (12) is the density gradient driving term. The function f_1 is always greater than zero, indicating that the density gradient is always destabilizing. The second term is the temperature gradient driving term. The function f_2 can be either negative or positive depending on whether the temperature gradient is stabilizing (Pfirsch Schliiter regime according to our rule of thumb), or destabilizing (plateau and banana regime). The third term is the ion-ion collisional damping. We use polynomial approximations for f_1, and f_2, which are discussed fully in Appendix A. Then, from Eq. (13), we can solve for the critical shear, Θ_{cr}, for

each $k\rho_i$. Once Θ_{cr} has been determined we have everything needed to advance the fluid quantites a time step.

In our computation Eqs. (11) and (12) were solved for five values of $k\rho_i$. These values were $k\rho_i = 0.25,\ 0.5,\ 0.75,\ 1.0,\ 1.25$. In order to determine the fluctuation level, $e\phi/T_e = \delta n/n_o$, we simply see what fluctuation level is required to produce the necessary transport. The quasi linear expression for the thermal conductivity is

$$K_{an} = \sum_k \frac{20}{3\pi} k^2 \frac{|\phi(k)|^2 c^2 \sqrt{2\epsilon}}{B_o^2 T_e} I_m \left\{ \left\langle \frac{1}{4} \frac{m v^2 (m v^2/T_e - 3)}{\omega + i\nu_{ef} - \omega_d} \right\rangle \right\} \tag{14}$$

where the triangular brackets mean an average over the magnitude of the particle velocity. Thus from the known value of K_{an} and $k\rho_i$, a fluctuation level may be calculated.

The Density Response

Although we only solve for the temperature profile with an assumed electron density profile, it is possible to solve for the density profile also. The resulting calculations however would be much more involved for at least two reasons. First of all, using a specified density profile for all time greatly simplified the numerics involved in the solution of the dispersion relation. Secondly, to solve for the density, one must include all sources of electrons. This means solving the coupled system of ion, neutral, and impurity transport, and also utilizing reliable models for ion, neutral, and impurity recyclying at the walls.

However, in principle at least, it is not difficult to solve for the density the same way as we solve for the temperature. The density equation is

$$\frac{\partial n}{\partial t} = \frac{1}{r} \frac{\partial}{\partial r} r(D_{cl} + D_{an}) \frac{\partial n}{\partial r} + S \tag{15}$$

where D_{cl} is the neoclassical diffusion coefficient, S is a term for all sources and sinks of electron density from Ware Pinch, ionization and recombination of impurities, and ionization and recombination of neutrals. Approximate expressions for S can be found in the Princeton work. Finally D_{an} is the anomalous Diffusion coefficient

$$D_{an} = \alpha' D_B \frac{q^{-n'}}{1 + q^{-n'}} + \alpha D_B \frac{(\Theta/\Theta_{cr})^{-n}}{1 + (\Theta/\Theta_{cr})^{-n}}. \tag{16}$$

In Eq. (16) above the factors α and α' result from the fact that the thermal conduction and diffusion coefficients are not the same. The quasi-linear theory of the trapped electron instability[24] gives a value for α. This quantity usually has a value less than, but of order unity, typically α is about one half or one third. (Actually, for the trapped particle instability the temperature gradients can drive particle fluxes and the density gradients can drive energy fluxes. These effects could also be included in Eqs. (1) and (15).) An expression for α' would have to come from the theory of the MHD instabilities occurring near the $q = 1$ surface in the center of the tokamak.

To summarize, it is possible to extend the work presented here to include the density response as well as the temperature response. Whenever the plasma is unstable, anomalous diffusion is turned on and the density profile will quickly relax. The anomalous diffusion coefficient is then related to the anomalous thermal conduction coefficient by the quasi-linear theory of the relevant instability.

The Dependence of the Temperature Profile on the Density Profile and Exponent of the Thermostat Function

In this subsection and the next few subsections we describe a series of tests of the code. For all tests, we have used PLT parameters in experimental runs recently reported[37]. These are $R = 135$ cm, $a = 45$ cm, $q(a) = 4.6$, $B = 35$ KG, $Z_{ef} = 4$ and $n(r = 0) = 5 \times 10^{13}$ cm $^{-3}$. The first run used exponents $n = 8$, $n' = 20$ and a density profile $n = n_o(1 - 0.85\ (r/a)^2)$. The steady state electron temperature is shown in the dashed curve of Fig. 1. Clearly, there is a very large unstable region of the plasma, extending nearly to the edge. The density profile we have chosen is so unstable that no amount of shear consistent with $q(0) = 1$, $q(a) = 4.6$ can stabilize it. Thus the temperature gradient flattens out over a very wide region and the heat flux is characterized by Bohm diffusion. Finally, near enough to the edge, the plasma is linearly stable and the diffusion is classicial, but with a very large temperature gradient. This result and the physical model used to derive it are obviously unphysical for a number of reasons. First of all, an electron temperature of 2 KEV so near the limiter is almost certainly unphysical. Second, it is not clear how accurate the numerics are for such a profile; there are only two grid cells in the steep temperature drop region at the edge (although the final steady state solution does remain constant in time). Third, and most important from our point of view, the density profile is assumed frozen into a very unstable shape. The instability will in fact relax this density profile, as discussed in the previous subsection. Since our code does not allow the density profile to relax, we have tried another run with the same density profile, but where the density profile cannot itself drive instability. That is we have set $f_1 = 0$, but with all density gradient effects (for instance drift resonances) included in f_2. In a very crude way, this mocks up the fact that the density gradient has relaxed and can no longer drive the instability. The resulting electron temperature profile is shown as the dash dot curve in Fig. (1). Notice that the temperature profile now looks much more resonable and physical. The fact that the temperature peak is somewhat higher is also resonable since the profile is now more stable.

As a final example of the effect of density profile on temperature, we ran the code with a more stable density profile $n = n_o(1 - 0.5\ (r/a)^2)$. The result is shown in Fig. 1 as the solid curve. Since this seems to be the most reasonable temperature profile, in all our subsequent runs, we used this density profile and retained f_2 in the dispersion relation.

The next thing to examine is the dependence of the result on the exponent of the thermostat function. Clearly, as $n \rightarrow \infty$ the temperature profile will be independent of n. Actually the shape of the thermostat function depends upon the nonlinear theory of the instability. It may be that the effect of nonlinear theory (as manifest in the shape of the thermostat function) plays an important role. For our purposes , we neglected this aspect of the anomalous transport and chose an n large enough that the temperature profile is independent of n. The steady state temperature profiles for 3 different values of n, $n = 4$, 16 and 32 are shown in Fig. 2. (The temperature profile for $n = 8$ is shown in Fig. 1). Notice that the result for $n = 4$ gives a somewhat lower temperature than the results for $n = 16$ and 32. The reason is that in both cases, the thermal conduction is a very small fraction of the Bohm value. However for $\Theta < \Theta_{cr}$, the thermostat function for $n = 4$ is larger than that for $n = 32$, so the thermal conduction is greater and the temperature should be smaller. Henceforth, we retained the choice $n = 32$ in all runs.

As a final check on the results of the code, we have taken the solid temperature profile of Fig. 1 and have numerically solved the full linear dispersion relation, Eq. (9), at 4 points on this profile. The numerical solution of the dispersion relation confirmed that the profile is marginally stable. At the points in the profile where the Θ thermostat function is zero, the numer-

ical soulution of Eq. (9) showed no instability. At the points where the Θ thermostat function is greater than zero, the numerical solution of Eq. (9) showed a very slighly growing or damped roots. The plasma therefore is very close to marginal stability.

Classical Versus Neo-Classical Resistivity

One possible question is whether to use the classical expression for conductivity or the neo-classical expression

$$\sigma_{NC} = \sigma (1 - (1.9 (r/R)^{1/2} - r/R)/(1 + \nu_e^*)). \tag{17}$$

In Figs. 3a and b are shown plots of electron temperature profile and $q(r)$ profile for the use of classical and nonclassical resisitivty. Notice that the temperature profiles for the two are quite similar. However the q profiles are strikingly different. For the case of classical resisitivity q is everywhere above one. For the case of non-classicial resisitivty, q sinks to values considerably smaller than one.

The reason is that for the case of classicial resisitivity, the resistivity depends only on temperature, so that flattening the temperature profile flattens the current profile. For neo-classicial resisitivity however the resisitivity depends on both temperature and radius. Thus flattening the electron temperature profile (which is all that anomalous thermal conduction can do) does not flatten the current profile. Thus the instability is not reacting back directly on the driving mechanism. (We are not sure how to interpret this result. If there is a strongly exicted internal kink or tearing mode in the center, the magnetic field lines will almost certainly not stay on smooth circular magnetic surfaces, but rather will more likely wander ergodigally throughout the region $q < 1$. It is not at all clear to us whether neo-classical expressions for resisitivity are valid in this case. Possibly, the neoclasical expression for resisitivity should be averaged in some way over the $q < 1$ region. We have decided to avoid this problem by using the ordinary classical expression for conductivity (Eq. (2)) so that anomalous thermal conduction alone flattens out both the temperature and current profile. However this question may be worth additional study.)

Dependence on Shear Damping

Recently there has been some speculation [31,35,36] to the effect that because of coupling of different mode rational surfaces, shear is not as effective a damping mechanism as indicated in the linear dispersion relation Eq. (9). We have run the code with the shear induced damping reduced by a factor of two ($\Theta \rightarrow \Theta/2$ in Eq. (9)). The plot of electron temperature is shown in Fig. 4. Notice that the central temperature drops from about 3.2 KEV to about 2.4 KEV. In all our subsequent runs, we retain this choice, $\Theta \rightarrow \Theta/2$, in Eq. (9).

The Energy Confinement Time

As will be shown in the next section, our code generally gives good agreement with experiment on central temperature and temperature profile, but not nearly as good agreement on the energy confinement time τ_E. The reason is the extreme sensitivity of τ_E on relevant parameters for ohmically heated tokamaks. The energy confinement time is defined as the energy content divided by the power into the tokamak IV (current times voltage),

$$\tau_E = \frac{\int d^3r\, 3/2\, n(T_e + T_i)}{IV} \tag{18}$$

Let us call the central temperature T_0 and the temperature half width $\Delta r(T)$. Then the energy content scales as $T_0\, \Delta r^2(T)$.

In our code, only the current is specified, the voltage must be calculated from the resisitivity profile. The conductivity scales as $T_o^{3/2}$ and the total resistance scales as $\Delta r^{-2}(T)$. Thus the voltage scales as $T_o^{-3/2}\ \Delta r^{-2}(T)$. Hence the theoretical energy confinement time scales as

$$\tau_E(Th) \sim T_o^{5/2}\ \Delta r^4(T). \tag{19}$$

Thus a fifteen percent error in T_o and $\Delta r(T)$ implies an error of more than a factor of two in τ_E. This sensitivity of τ_E is characteristic not only of our code, but is also characteristic of any code which attempts to calculate temperature profiles of ohmically heated tokamaks with specified current.

It might be argued that such a sensitivity is also true of experimental determinations of τ_E. While there are experimental uncertainties in T_o and $\Delta r(T)$, an experimentalist at least has an accurate measure of the voltage. Thus experimentally, the confinement time scales as

$$\tau_E(EX) \sim T_o\ \Delta r^2(T), \tag{20}$$

which exhibits much less sensitivity to the temperature and temperature profile than the scaling shown in Eq. (19). Thus we conclude that relatively inaccurate predictions of τ_E for ohmically heated tokamaks is something transport codes must live with.

Summary

To summarize, we assume in all subsequent runs the density profile $n = n_o(1 - 0.5\ (r/a)^2)$, classical rather than neo-classical resisitivty, $n' = 20$, $n = 32$, and that the shear damping is reduced by a factor of two. For PLT parameters $R = 135$ cm, $a = 45$ cm, $q(a) = 4.6$, $B = 35$ KG, $Z_{ef} = 4$, $n_o = 4.2 \times 10^{13}$, and a hydrogen plasma is assumed, the prediction of our code is shown in Fig. 4. Plotted are electron and ion temperature, $q(r)$ and the radial dependence of the q and Θ thermostat functions. The confinement time (electron plus ion) is 200 miliseconds. Clearly the inner region is marginally stable to the internal kink mode, the region between $r/a = 0.25$ and $r = 0.9$ is marginally stable to the trapped electron instability, and the outer most region is classical.

III. Results for TFR

One very interesting experimental result from TFR [21] is that the temperature half width $\Delta r(T)$ depends on only a single parameter, $q(a)$, even though two parameters, B and I are independently varied. This result comes out of our original simplified marginal stability theory [8]. There the driving term for instability depended only on η_e and τ, while the shear stabilization term depended only on Θ and r. Only the relative temperature profile was solved. However, in the simplified theory, the only parameter characterzing the relative temperature profile was $q(a)$. Thus $\Delta r(T)$ depended only on $q(a)$; the larger $q(a)$, the more peaked the temperature profile. Although we now use a much more complicated dispersion relation, the same basic result still holds true. In Fig. 5 is shown (solid line) the predictions by our code for $\Delta r(T)$ as a function of $q^{-1}(a)$.

Here we have assumed $Z_{ef} = 3$ and $n_o = 6 \times 10^{13}$, and a helium plasma was assumed since most of the experiments in Ref. 21 used a helium plasma. Various dots show the calculated points. Although there is some scatter to the points, $\Delta r(T)$ basically does depend on the single parameter $q(a)$. The dashed line shows the experimental result from TFR. Note that

our code predicts somewhat wider temperature half widths than are measured. A possible reason for this discrepancy is the effect of radiation. This will be discussed qualtatively shortly.

Another interesting result from the TFR experiment is that the position of the $q = 1$ surface, as defined by the radial position of the mode in the saw tooth oscillations in the soft X/ray signal, also depends only on the single parameter $q(a)$. In Fig. 5, the dash dot line shows that the predicted value for the $q = 1$ surface, as defined by the radial position where the q thermostat function drops to half its maximum value, also depends principally on this single parameter.

In Fig. 6a and b are predictions of the code for electron temperature compared to experiment[21], for three discharges. The predicted energy confinement times (electron plus ion) are $\tau_E = 65, 96, 108$ ms. for the 3 cases $B = 25, 40$ and 50 Kg. These are larger than the experimental values by about a factor of 5. Notice however that the code does give good agreement with experiment as regards central temperature. In Fig. 7 are plotted the radial dependence of T_e, Ti, q, for the run with $B = 50$ Kg, $I = 140$ KA.

Other quantities of interest are the $k\rho_i$ of the fluctuation and predicted values of $e\phi/T_e$ as a function of radius. These are shown in Fig. 8 for a discharge with 60 KG, 300 KA. The fluctuation level seems to be comparable to, but somewhat larger than recently reported[38 –40]. Actually the values for $e\phi/T$ given in Ref. 38 should be doubled[40]. Notice that the discontinuities in $e\phi/T$ with r come about at the position where the $k\rho_i$ of the mode jumps. If we could have assumed a continuous spectrum in k, $e\phi/Te$ would surely be a continuous function of r.

We now discuss what effect impurity radiation would have on the temperature profiles. Experiments on TFR have shown that a large fraction of the input ohmic power is radiated away by impurities[38]. The light impurities, typically Oxygen, radiate away the largest share of the power, and this radiation comes from the edge regions of the plasma, in the center the Oxygen is fully stripped[41,42] and there can be no line radiation. The heavy impurities, typically molylduim radiate away a smaller fraction of the power and this radiation comes from the central hot region of the plasma. The radiation is still line radiation; molylduim is not fully stripped until the plasma reaches a much higher temperature.

We will first discuss the impurities near the center where there is anomalous tranport. Our basic hypothesis is that in the marginally stable regime, the plasma picks the marginally stable profile nearly independently of the driving mechanism. Thus if there is an additional energy loss term, the plasma will still remain at a marginally stable temperature profile, but the thermal conduction and fluctuation level will decrease. However if the number of impurities is so great that classical conductivity alone is sufficient to maintain a stable profile, then clearly this profile cannot be maintained. If the number of impurity ions is larger than this critical value, the temperature should drop. Thus in the regions where there is anomalous transport a tokamak electron temperature profile should be relatively insensitive to the presence of impurities as long as the number of impurities is sufficiently small. For larger concentrations of impurities, the electron temperature should drop sharply as the impurity concentration increases.

We conclude this section with a discussion of the effects of impurity radiation for plasmas whose edge region is classical. If the edge region of the tokamak is classical, and the electron and ions are nearly equilibrated ($T_e = T_i \cong T$), and there is no radiation loss or energy deposition in the edge region, Eqs. (1) in the edge region can be reduced to

$$r K_{ci} \frac{\partial T}{\partial r} = constant. \tag{21}$$

Above we have made use of the fact that $K_{ci} >> K_{ce}$. Since the ohmic energy channels into the hotter regions, it is reasonable to assume no energy deposition in the edge region. Equation (21) simply states that the total energy flux through each cylinder is constant, and is equal to the Ohmic input energy. If there are losses due to radiation (or charge exchange, etc.), then the energy flux in the outer region must be smaller because some of the ohmic input power has been radiated away before it reaches the edge. This then implies that $\frac{\partial T}{\partial r}$ will be smaller at each temperature in the classical region, and thereby $\Delta r(T)$ will decrease.

IV. Results for Alcator

Perhaps the most striking experimental result for Alcator is the increase of energy confinement time with density[43,44]. Our code does predict this basic dependence, although as with TFR, the actual confinement time is too large, this time by about a factor of three. In Fig. 9 is shown the dependence of energy confinement time on central density for three choices of field and current, $B = 50$ KG, $I = 100$ KA; $B = 75$ KG, $I = 100$ KA; and $B = 75$ KG, $I = 150$ KA. In all cases, $Z_{ef} = 1$ and we used a hydrogen plasma. Notice that for central densities less than about 2×10^{14} cm $^{-3}$, the confinement time increases roughly linearly with density. For larger n_o the confinement time begins to decrease again.

Apparently what is happening is that as long as a region of the plasma is goverened by anomalous tranport, the central temperature and temperature half width are relatively independent of density. Then the power input is independent of density, since the resisitivity depends only on temperature. The energy content however is proportional to density, so that the energy confinement time is proportional to density. When the density is sufficiently high however, the plasma is in the Pfirsch Schluter regime, and there is no trapped particle instability. Then the energy confinement time begins to decrease with density. For all three choices of current and field, the points with $n_o = 5 \times 10^{14}$ were completely stable. Not only are there no trapped particle instabilities in the region of maximum gradient, q was everywhere larger than one so that are no MHD modes in the center either. Apparently the largest confinement time occurs just on the transition from anomalous to classical thermal conduction. The highest electron temperature however are in the regime of anomalous thermal conduction and low confinement time. In Fig. 10 a and b are plotted the radial dependence of T_e and T_i for different densities for the case $B = 75$ KG, $I = 100$ KA. Notice that at low density, where the thermal conduction is anomalous, the temperature profiles are quite peaked. At higher density, where the thermal conduction is classical, the temperature profiles are quite broad.

V. Results for ATC

Since fluctuation spectra were measured in ATC[45], we have run our code for an ATC plasma in the uncompressed state. The parameters are $B_o = 16$ KG, $I = 65$ KA, $n_o = 1.4 \times 10^{13}$, $Z_{ef} = 2$. A plot of electron temperature, ion temperature and q as a function of radius is shown in Fig. 11. In Fig. 12 a and b are shown the radial dependence of $k\rho_i$ and $e\phi/T_e = \delta n/n_o$. Typical values of $e\phi/T_e$ 10^{-2} are consistent with values measured by microwave scattering in Ref. 45.

VI. Conventional and Unconventional Approaches to Electron Heating

Since Ohmic heating has not heated the electrons in a tokamak plasma to more than about 2.5 Kev, it is generally agreed upon that some sort of supplementary heating is necessary

to reach reactor temperatures. Currently, people are investigating heating by microwave and neutural beams. The obvious hope is that by, say, doubling the input power one can double (or more than double) the plasma temperature. For our purposes here, we define as conventional heating such schemes which rely on increasing the input power.

However there are two sides to the heating problem, the energy input and the power losses. If the ion losses are classical, as assumed here, then there is no way they can be reduced. The electron losses however are anomalous. If there is anyway these losses can be reduced, the electrons will heat. Furthermore they will heat without additional input power, so the confinement time will increase. (Actually, controlling the losses probably requires input power also). We will define as unconventional heating such schemes which rely on controlling the electron losses. The situation is rather like a phase change[8]. If water is just at the boiling point, putting in excess energy does not raise its temperature. However raising the boiling point does allow the water to be heated to higher temperatures. The problem with heating by controlling losses is, of course, that there is now no general agreement on what causes these losses, much less on how these losses can be controlled. Nevertheless, at least our model of the anomalous losses shows that there is a great deal to be gained if one can control them.

In this section we discuss one conventional heating scheme and three unconventional heating schemes. All runs are done for TFR with $I = 140$ KA and $B = 50$ KG. The results are summarized in Table 1.

The first heating scheme we examine is heating of the plasma by neutural beams. We have performed two runs. The first of these runs doubled the total Ohmic power by depositing 38 KW of beam power into the ions and another 38 KW into the electrons. The deposition profile is uniform as a function of radius. As is shown in Table 1 the central electron temperature increases from about 2.5 Kev to about 2.8 Kev. The confinement time however decreases from 108 ms to 74 ms. To examine the effect of more beam power and a better deposition profile, we have done another run tripling the original Ohmic power to 76 KW deposited in ions and 76 KW in electrons and choosing an energy deposition profile proportional to the density profile. The central electron temperature now rises to 3 Kev, but the confinement time decreases to 59 ms.

One can understand these results very simply. As more power is injected into the plasma, the temperature gradient tends to increase and the plasma tends to be pushed further into the plateau and banana regime. Thus the plasma is driven into a more unstable state. However, as the plasma is pushed into a more unstable state, it is fighting the thermostat function, which pushes it back toward stability. The harder the plasma is pushed toward instability, the harder it fights back. Thus, according to our theory, increasing the input power into the electrons is not a particularly effective way to heat the plasma.

It is now worth while to compare these results with experimental results of beam injection in TFR[15]. A quantitative comparison is difficult because the confinement times we calculated for ohmically heated tokamaks were too large by about a factor of five. Correspondingly, the Ohmic power input was too small by somewhat less than this factor. These are some qualitative comparisons that can be made however. The input beam power into TFR was also comparable to or larger than the Ohmic input power, and the power deposition was about half into electrons and half into ions. The observed ion temperature increased by about 1 Kev. Our code showed a considerably smaller increase in T_i (the central ion temperature only increased by about 200 ev). The reason is that the ions are in the Plateau regime where the thermal conductivity is an increasing function of temperature. However, once the ions are heated to

the banana regime, where the thermal conductivity is a decreasing function of temperature, significant heating ion should result with increasing input power. We attribute the disagreement between the computed and experimental ion temperature to the fact in the experiment, much more power is going into the ions from the beams. Thus the ions can be heated up to the banana regime. Additional ion heating then requires much less beam power.

One very intesting result however is that in the experiment, the electrons either do not heat at all, or else heat by no more than 10%. Figures 8 and 13 of Ref. 15 show electron temperature before and during injection, and there is very little difference. It appears that the thermostat function controlling the experimental temperature profile in TFR has an even harder onset than the thermostat function we have been using, Eq. (7), with $n = 32$.

We now discuss three unconventional heating schemes. First, let us imagine that some way could be found to stabilize the MHD instability at the $q = 1$ surface. Since this is a large scale instability, this may possibly be done with feedback or dynamic stabilization. It is interesting to note that dynamic stabilization has recently been shown to be possible for the Raleigh-Taylor instability in a laser produced plasma[46]. While we do not know if dynamic stabilization of internal kink and tearing modes is possible, our results show that it is worth additional investigation.

In our numerical simulation, we have not assumed complete stabilization of MHD modes, rather we have assumed that it is the $q = 1/2$ surface which is unstable rather than the $q = 1$ surface. The result, as shown in table 1, is a very impressive amount of heating. The central electron temperature is increased to 4.4 Kev and the confinement time increases to 425 ms. Apparantly what is happening is that decreasing $q(0)$ by a factor of two increases the allowed shear by about a factor of two. (Recall that the shear is related to the change in $1/q$.) The increased shear then allows for larger electron temperature gradients before reaching the threshold for instability.

Another way to reduce the electron losses is to artificially increase the collisionality of the electrons. At least one way to do this is to bathe the plasma in microwaves at the electron cyclotron frequency[47]. This will cause enhanced pitch angle scattering of the electrons. Thus the temperature at which the electrons enter the plateau and banana regime is raised, so that a larger part of the plasma cross section will be stable. Since the pitch angle scattering is caused only by the microwave power, and not by an electron-ion scattering, the plasma resistivity will be unaffected, so there will be no additional energy input caused by an anomalous resistivity.

We have done a numerical simulation in which the collisionality in the dispersion relation and electron thermal conductivity are increased by a factor of 2.5, but where the collisionality in the resisitivity is unchanged. The results are shown in Table 1. The central electron temperature increases to 2.9 Kev and the energy confinement time increases to 145 ms.

If this interpretation is correct, it implies that heating experiments at the electron cyclotron frequency will do as well or better by injecting power with a spectral width $\Delta\omega/\omega \sim 2a/R$, instead of a single frequency chosen to match the cyclotron frequency at a particular point. Such a spectral width would allow for the electron collisionality to be increased across the entire plasma cross section.

As a final example of the control of electron losses, we will discuss shaping the plasma cross section. It has recently been shown that an elliptical cross section both slightly increases the shear induced damping[48] and reduces the trapped particle induced growth[49,50]. While our

code is not capable of handling elliptical cross sections, we mock up the effect of ellipticity by increasing the (reduced, See Sect. IIG) shear induced damping by a factor of 1.3 and reducing the trapped particle induced growth rate by a factor of two. This corresponds roughly to an ellipticity of three[48 -50]. As is shown in table 1, the central electron temperature increases to 2.95 Kev and the energy confinement time increases to 142 ms. It should be restated now that in all three unconventional heating schemes, the power used to reduce the electron thermal conductivity was not figured in the definition of confinement time. The reason is that we do not know what this power is. Surely power is needed to stabilize the $q = 1$ surface or to increase the electron collisionality with microwaves at the electron cyclotron frequency. Shaping the cross section, however, should require no additional power.

To summarize, we have shown that conventional heating is possible, but that the confinement time (or at least the electron confinement time in experiments) is normally reduced. However heating by controlling the anomalous losses offers a potentially very attractive way to heat the electrons in tokamaks.

VII. Conclusions

Our conclusion is that marginal stability theory is a very useful approach to the problem of electron energy confinement in tokamaks. At the least this theory provides a worst case analysis of the anomalous thermal transport resulting from a given instability. It predicts an energy confinement time scaling will density, as seen in Alcator; and it also shows that the temperature half width $\Delta r(T)$ and the radius of the $q = 1$ surface depends only on the single parameter $q(a)$, as seen in TFR. Also, it provides very natural explanations for the failure to heat electrons with neutural beams in TFR and also for the heat pulse propagation experiments in ORMAK. Finally, it suggests that controlling the electron losses may be a more effective approach to electron heating than injecting additional power.

Acknowledgment

This work was supported by ERDA. We would like to thank Jay Boris, Edward Ott and K. R. Chu for a number of useful discussions.

REFERENCES

1. P.H. Rutherford and D.F. Duchs, Nucl. Fusion **17**, 565 (1977), and Princeton Matt report 1272, August 1976, Princeton University, Princton N. J.
2. D.F. Duchs, H.P. Furth, and P.H. Rutherford in Plamma Physics and Controlled Nuclear Fusion Research (Proc. 4th Int. Conf., Madison, 1971) 1, IAEA, 425 (1971).
3. C. Mercier, Soubbaramayer and J.P. Boujot in Plasma Physics and Controlled Fusion Research (Proc. 4th Int. Conf. Madison, 1971) 1, IAEA, 369, (1971).
4. D.F. Duchs, H.P. Furth and P.H. Rutherford, Nucl. Fusion **12**, 341 (1972).
5. Y.N. Dnestrovskii and D.P. Kostomarov, Sov. At. Energy **29**, 1205 (1970).
6. Y.N. Dnestrovskii, D.P. Kostomarov and N.L. Pavlova, Princeton Plasma Physics Laboratory Report Matt - Trans - 107 (1971).
7. M.M. Widner, R.A. Dory and J.T. Hogan, Phys. Letters **36A**, 217 (1971).
8. W.M. Manheimer and Jay P. Boris, Comments on Plasma Physics **3**, 15 (1977).
9. W.M. Manheimer, K.R. Chu, E. Ott, and J.P. Boris, Phys. Rev. Lett., **37**, 286 (1976).
10. W.M. Manheimer and J.P. Boris, Phys. Rev. Lett., **28**, 659 (1972).
11. J.P. Boris, J.M. Dawson, J.H. Orens and K.V. Roberts Phys. Rev. Lett., **25**, 706 (1970).
12. J.P. Christainsen and K.V. Roberts, *Second European Conference on Computational Physics*, IPP Garching, 27-30 April, 1976.

13. C.F. Kennel and H.E. Petchek, J. Geophysical Res. **71**, 1 (1966).
14. E. Minardi, Phys. Fluids 16, 122 (1973).
15. Equipe T.F.R., IAEA Conference, October 1966, Berchesqarten, Germany Papes IAEA CN35/A4-2.
16. J.D. Callen and C.L. Jahns, Phys. Rev. Lett., **38**, 491 (1977).
17. T.M. Antonsen and E.Ott, Presented at the Third International Conference on Theoretical and Experimental Aspects of Heating of Toroidal Plasmas. Grenoble, France, June 28 - July 2, 1976.
18. P.H. Rutherford, H. P. Furth and M.N. Rosenbluth, Plasma Physics and Controlled Fusion, IAEA Vienna Vol. 1 p. 533.
19. R.B. White, D.A. Monticello, M.N. Rosenbluth, H.R. Strauss and B.B. Kadomtsev in Plasma Physics and Controlled Fusion, IAEA Vienna, 1971, Vol. 1, 495.
20. Von Goeler, W. Stokiek, and N. Sauthoff, Phys. Rev. Lett., **33**, 1201, (1974).
21. Equipe T.F.R. Behavior of Discharges and Internal Disruptions in TFR, VIIth European Conference Plasma Physics Sept. 1-5, 1975 Lausanne, Switzerland.
22. B.B. Kadomtsev and O.P. Pogutse, Sov. Phys. JETP **24**, 1172 (1967).
23. T.H. Dupree, Phys. Fluids **10**, 1049 (1967).
24. W. Manheimer, K.R. Chu, E. Ott, J.P. Boris and J.D. Callen, Nucl. Fusion **16**, 203 (1976).
25. B. Cohen, J. Kromes, M. Rosenbluth and W. Tang, Physics of Fluids, to be published.
26. T.H. Dupree and D. Tetrault, Physics of Fluids to be published, also presented at Sherwood meeting, May 1977, San Diego, Cal.
27. P. Liewer, W.M. Manheimer and W.M. Tang, Phys. Fluids **19**, 276 (1976).
28. W.M. Tang, P.H. Rutherford, H.P. Furth and J.C. Adam, Phys. Rev. Lett., **35**, 660 (1975).
29. J.C. Adam, W.M. Tang and P.H. Rutherford, Phys. Fluids **19**, 561 (1976).
30. D. Ross, W. Tang, and J. Adam, Phys. Fluids **19**, 613 (1977).
31. G. Rewoldt, W. Tang, and E. Frieman, Phys. Fluids **19**, 402 (1977).
32. K.R. Chu and W.M. Manheimer, Nucl. Fusion to be published. See also NRL Memorandum Report 3336 (Aug. 1976).
33. A.A. Rukadze and V.P. Silin, *Sov. Physics - Uspekhi II* 659 (1969).
34. D. Pearlstein and H. Berk, Phys. Rev. Lett., **23**, 220, (1969).
35. W.M. Tang, Private Communication.
36. J.B. Taylor, IAEA Conference, October 1976, Berchesgarten, Germany Paper IAEA.
37. D. Grove, V. Arunasalam, K. Bol, D. Boyd, N. Bretz, M. Brusati, S. Cohen, D. Dimock, F. Dylla, D. Eames, H. Eubank, B. Fraenkel, J. Girard, R. Hawryluk, E. Hinnov, R. Horton, J. Hosea, H. Hsuan, D. Ignat, F. Jobes, D. Johnson, E. Mazzucato, E. Meservey, N. Sauthoff, J. Schivell, G. Schmidt, R. Smith, F. Stauffer, W. Stodiek, J. Strachan, S. Suchewer, S. von Goeler, K. Young, IAEA Conference, October 1976, Berchesgarten, Germany, Paper IAEA-CN-35/A2.
38. Equipe TFR, IAEA Conference, Berchesgarten, Germany, Oct. 1976. Paper number IAEA CN-35/A3.
39. F. Koechlin, V.G. Laude and J. How, Euratom Report EUR-CEA-FC-871, Fontenay-Aux-Roses, France.
40. F. Koechlin, private communication.
41. Equipe TFR, Nucl. Fusion, **15**, 1053 (1975).
42. J.E. Rogerson, J. Davis and V.L. Jacobs, J. Quant. Spectrosc. Radiat. Transfer, **17**, 343 (1977).
43. G.J. Boxman, B. Coppi, L.C.J.M. de Kock, B.J. H. Meddens, A.A.M. Oomens, L.Th.M. Ornstein, D.S. Pappas, R.R. Parker, L. Pieroni, S.E. Segre, F.C. Schuller, and R.J. Taylor, Presented at the VII European Conference on Plasma Physics, Lausanne, Switzerland, Sept. 1975.
44. E. Apgar, B. Coppi, A. Gondhalekar, H. Helava, D. Komm, F. Martin, B. Montgomery, D.

Pappas, R. Parker and D. Overskei, IAEA Conference on Controlled Fusion, Berchesgarten, Germany, Oct. 1976, Paper IAEA 35/A6.
45. R.J. Goldston, E. Mazzucato, R.E. Slusher and C.M. Surko, IAEA Conference on Controlled Fusion, Berchesgarten, Germany, Oct. 1976, Paper CN-35/A-11.
46. J.P. Boris, Comments on Plasma Physics 3, 1 (1977).
47. V.V. Alikaev, G.A. Bobrovskii, V.I. Poznyak, K.A. Razumova, V.V. Sannikov, Yu.A. Sokolov, and A.A. Shmarin, Sov. J. Plasma Physics 2, 212 (1977).
48. E. Ott, W. Manheimer and K.R. Chu, Phys. Fluids to be published; Also see NRL Memorandum Report 3516, May 1977.
49. E.Ott, K.R. Chu, and W.M. Manheimer, NRL Memorandum Report 3459, Feb. 1977.
50. K.R. Chu, E. Ott, and W. Manheimer, Phys. Fluids, to be published.

APPENDIX

The functions f_1 and f_2 defined in Sec. II contain contributions from the trapped and untrapped electrons,

$$f_1 = (1 - \zeta)\, Im\{T_1 + V_1\} \tag{A1}$$

$$f_2 = \zeta\, Im\{T_2 + V_2\}, \tag{A2}$$

where

$$V_1 = \int_U \frac{d^3\xi}{\pi^{3/2}} \frac{\exp(-\xi^2)}{(1 - \xi_{||} R_o)},$$

$$V_2 = \int_U \frac{d^3\xi}{\pi^{3/2}} \frac{\exp(-\xi^2)(\xi^2 - 3/2)}{(1 - \xi_{||} R_o)},$$

$$R_o = \nu_e/(Rq\omega) = \zeta\epsilon_n (2m_i/\tau m_e)^{1/2}/qb, \zeta = \omega_*/\omega,$$

$$T_1 = \int_T \frac{d^3\xi}{\pi^{3/2}} \frac{\exp(-\xi^2)}{1 + i R_1 \xi^{-3} - \zeta \epsilon_n \xi^2},$$

$$T_2 = \int_T \frac{d^3\xi}{\pi^{3/2}} \frac{(\xi^2 - 3/2)\exp(-\xi^2)}{1 + i R_1 \xi^{-3} - \zeta \epsilon_n \xi^2}$$

and

$$R_1 = \nu_e/(\epsilon \bar{\omega}) = 2\zeta \epsilon_n \nu_{e}^{*} (m_i\epsilon/\tau m_e)^{1/2}/qb.$$

U and T denote untrapped and trapped. An electron is considered trapped if $\xi_{||} < (2\epsilon)^{1/2}\zeta_|$ and $\xi > \nu_{*e}^{1/4}$. The first of these conditions defines the boundary of the loss cone in velocity space and the second condition results from demanding that the effective collision frequency for an electron is less than the bounce frequency in the magnetic mirror.

With this perscription of the trapped and untrapped regions of velocity space the imaginary parts of the untrapped integrals, V_1 and V_2 can be obtained by straight forward integration

$$Im\{V_1\} = \pi^{1/2} \exp(-R_o^{-2})[1 - \exp(-\nu_{*e}^{1/2})]/R_o$$

$$I_m\{V_2\} = \pi^{1/2} \exp(-R_o^{-2}) \left\{ \exp(-\nu_{*e}^{1/2}) \left[\frac{1}{2} - \nu_{*e}^{2} \right] - \frac{1}{2} \right\} / R_o$$

where we have assumed $R_o >> \epsilon^{-1/2}$.

The trapped integrals T_1 and T_2 can be further simplified by performing the indicated integration in spherical coordinates, $\int_T d^3\xi = 4\pi(2\epsilon)^{1/2} \int_{\nu_{*e}^{1/4}}^{\infty} \xi^2 d\xi$. Thus, the functions T_1 and T_2 contain a transcendental dependence on the three parameters ν_{*e}, R_1, and $\zeta\epsilon_n$.

We now show that setting the lower limit in the T_1 and T_2 integrals to zero gives a good approximation to these integrals for all ν_{*e}. If $\nu_{*e} > 1$ so that the lower limit of integration is significantly different from zero the value of R_1 will generally be quite large due to the square root of the mass ratio in the definition of R_1. Given that R_1 is large the integrals can be evaluated asymptotically for large R_1. For instance the asymptotic value of T_1 is found to be

$$T_1 \sim -i \frac{4}{\pi^{1/2} R_1} (2\epsilon)^{1/2} \exp(-\nu_{*e}^{1/4}) \left[1 + \nu_{*e}^{1/2} + \frac{1}{2} \nu_{*e} \right]. \tag{A3}$$

The explicit dependence of (A3) on ν_e is actually quite weak for $\nu_e \sim 1$. If $\nu_e >> 1$, in which case $R_1 >> 1$, and $T_1 \to 0$, even if the lower limit of integration had been chosen to be zero rather than $\nu_e^{1/4}$, both expressions are so small that either one gives a good approximation to the necessary shear. Thus, we ignore the explicit dependence of the integrals T_1 and T_2 on ν_e by setting the lower limit of integration to zero.

The remaining dependences of T_1 and T_2 on R_1 and $\zeta\epsilon_n$ were approximated by polynomials,

$$I_m\{T_1\} \frac{4}{\pi^{1/2}} (2\epsilon)^{1/2} \frac{E_1 - R_1^2}{1 + a_1 R_1 + b_1 R_1^2 + R_1^3} \tag{A4}$$

$$I_m\{T_2\} \simeq \frac{4}{\pi^{1/2}} (2\epsilon)^{1/2} \frac{E_2 + \beta R_1 + 1.5R_1^2}{1 + a_2 R_1 + b_2 R_1^2 + R_1^3} \tag{A5}$$

where a_1, a_2, b_1, b_2, and β are functions of $\zeta\epsilon_n$, and E_1 and E_2 are the limiting vaues of $I_m\{T_1\}$ and $I_m\{T_2\}$ as $R_1 \to 0$ which can be obtained exactly and depend on $\zeta\epsilon_n$.

The form of the polynomials and the dependences of a_1, b_1, a_2, b_2, and β on $\zeta\epsilon_n$ were chosen by comparison with numerically integrated values of T_1 and T_2. It can be seen that the approximations (A4) and (A5) agree with the actual values of T_1 and T_2 for both large and small R_1. By careful choice of the a's and b's we were able to get agreement within 10% between the polynomials and numerically integrated values of T_1 and T_2 for the relevant parameter ranges of R_1 and $\zeta\epsilon_n$.

The vaues of these parameters are

$$E_1 = \frac{1}{2} \pi \exp(-(\zeta\epsilon_n)^{-1})/(\zeta\epsilon_n)^{3/2}, \tag{A6a}$$

$$E_2 = -\frac{1}{2} \pi \left(\frac{3}{2} - (\zeta\epsilon_n)^{-1}\right) \exp(-(\zeta\epsilon_n)^{-1})/(\zeta\epsilon_n)^{3/2}, \tag{A6b}$$

for all $\zeta\epsilon_n$. The vaues of β, a_1, a_2, b_1 and b_2 are

$$\beta = 3.17 - 7.26\zeta\epsilon_n \tag{A7a}$$

$$a_1 = 0.0, \tag{A7b}$$

$$b_1 = 2.66 + 7.56(\zeta\epsilon_n), \tag{A7c}$$

$$a_2 = 11.18 (\zeta\epsilon_n)^{2.73}, \tag{A7d}$$

and

$$b_2 = -8.45 + 38.44 (\zeta\epsilon_n), \tag{A7e}$$

if $\zeta\epsilon_n > 0.64$ and

$$a_1 = -1.7 + (3.4 - 2.65(\zeta\epsilon_n)/(1 + 570(\zeta\epsilon_n)^4), \tag{A8a}$$

$$b_1 = 2.0 + 48.58 ((\zeta\epsilon_n) - 0.2)^2/((\zeta\epsilon_n) + 0.72), \tag{A8b}$$

$$\beta = -7.20 - 5.71(\zeta\epsilon_n) + (4.67 + 20.6(\zeta\epsilon_n))/(1 + 3.58(\zeta\epsilon_n)^3), \tag{A8c}$$

$$a_2 = 0.98/(\zeta\epsilon_n) + 1.5, \tag{A8d}$$

$$b_2 = 48.70(\zeta\epsilon_n)^{2.52} + 0.0025/(\zeta\epsilon_n)^{2.4}, \tag{A8e}$$

for $\zeta\epsilon_n < 0.64$.

Table 1

Scheme	Added Power Input	$T_e(0)$	τ_E
Only Ohmic, P = 76 kw	None	2.5 kev	108 ms
Beam, Uniform Deposition	38 kw into ions, 38 kw-electrons	2.8 kev	74 ms
Beam, Deposition	76 kw-ions 76 kw-electrons	3 kev	59 ms
Stabilization of $q = 1$	?	4.4 kev	425 ms
Increasing Electron Collisionality By 2.5	?	2.9 kev	145 ms
Cross Section Shaping	None	2.95 kev	142 ms

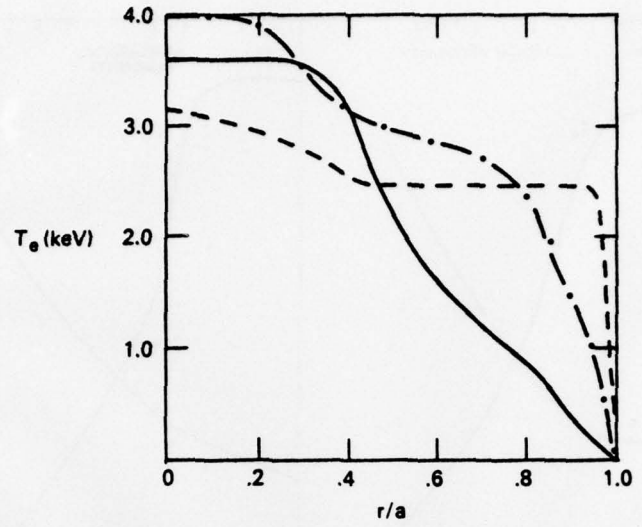

Fig. 1 – PLT electron temperature profiles; solid line, full dispersion relation $n = n_0(1 - .5\, r^2/a^2)$; dashed line, full dispersion relation $n = n_0(1 - .85\, r^2/a^2)$; dash-dot line modified dispersion relation $n = n_0(1 - .85\, r^2/a^2)$

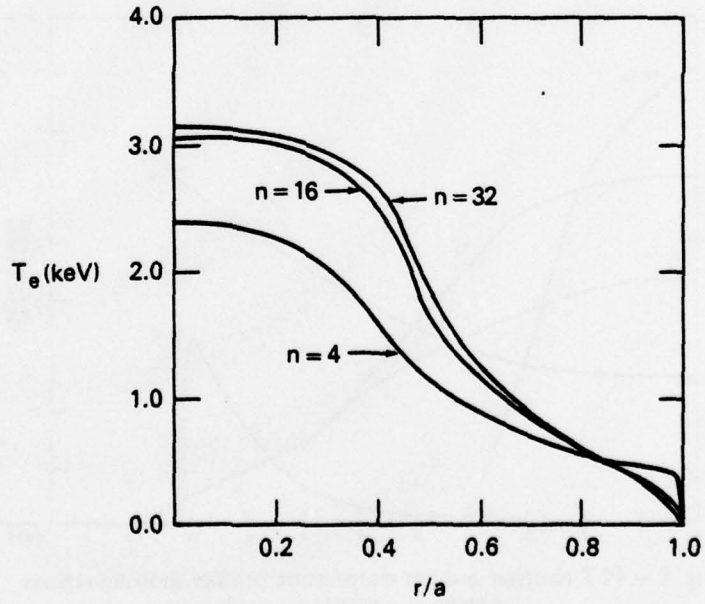

Fig. 2 – PLT electron temperature profiles for various values

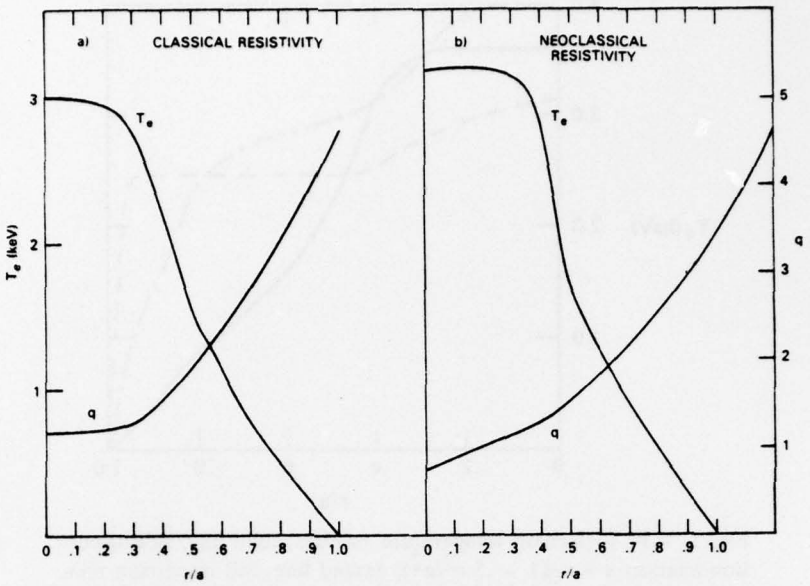

Fig. 3 – PLT electron temperature profiles obtained with (a) classical and (b) neoclassical resistivity

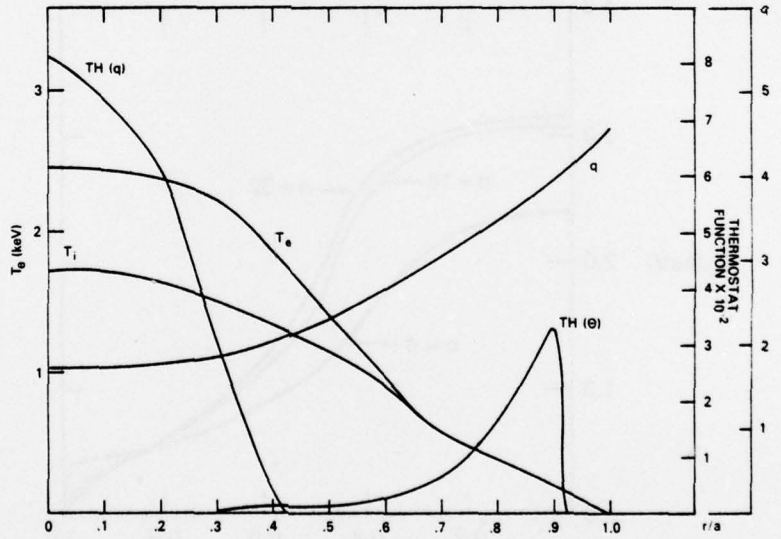

Fig. 4 – PLT electron and ion temperature profiles showing regions of MHD and DTEM instability

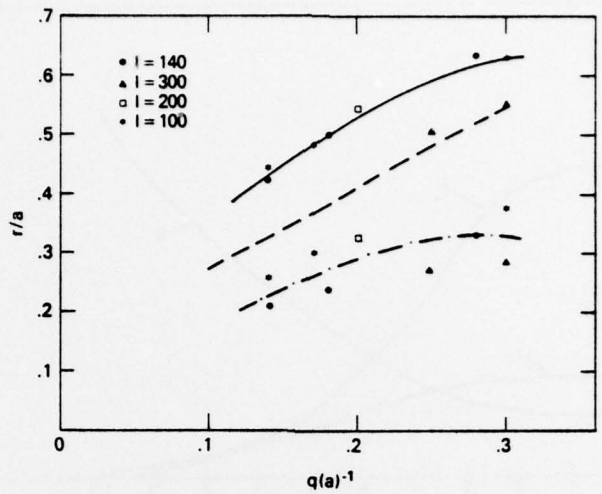

Fig. 5 – Temperature half-width and width of the $q(r) = 1$ region in TFR as a function $q(a)^{-1}$. The solid and dash-dot line are approximate fits to the numerically obtained data points. The dashed line is the experimentally observed temperature half-width.

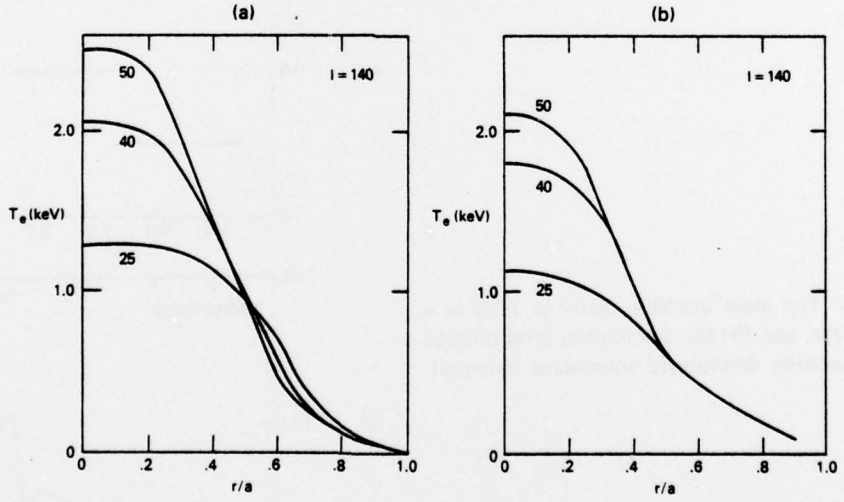

Fig. 6 – Electron temperature profiles in TFR. (a) numerically obtained (b) experimentally obtained

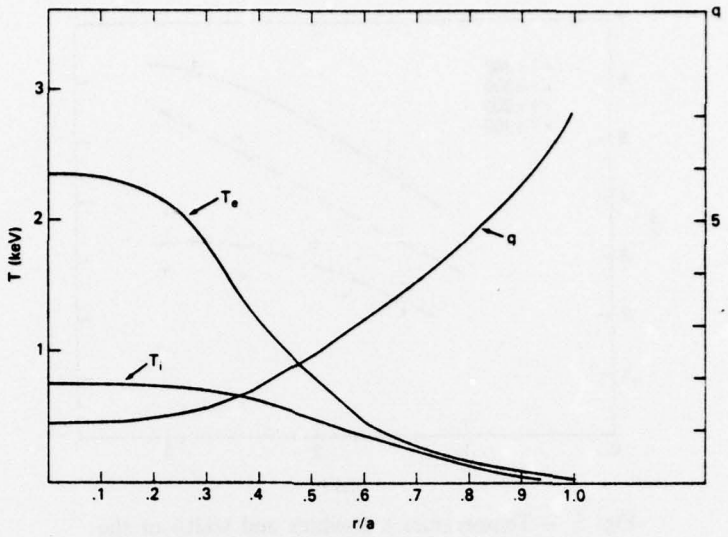

Fig. 7 – TFR electron and ion temperature profiles

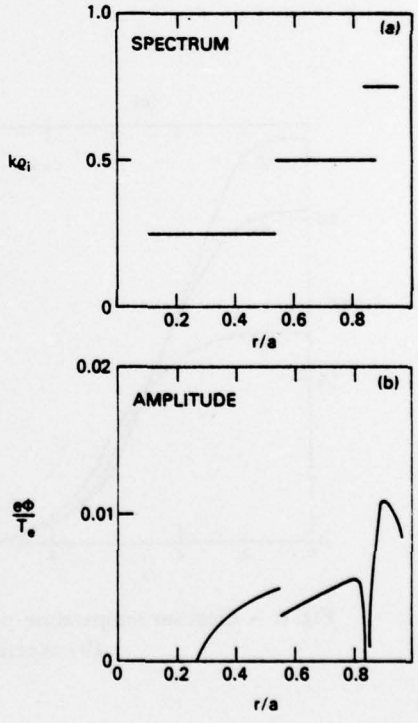

Fig. 8 – (a) The most unstable mode in TFR as a function of r/a, and (b) the fluctuation level implied by the numerically determined anomalous transport

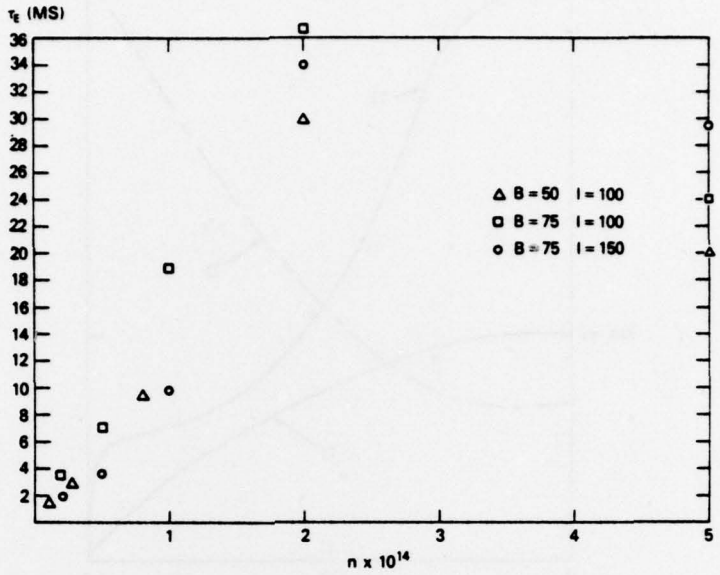

Fig. 9 – Energy confinement time versus central density in Alcator

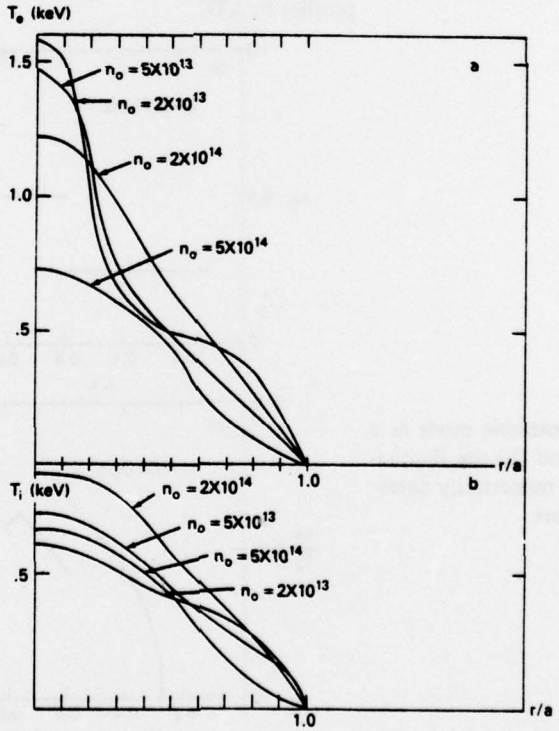

Fig. 10 – Electron and ion temperature profiles in Alcator

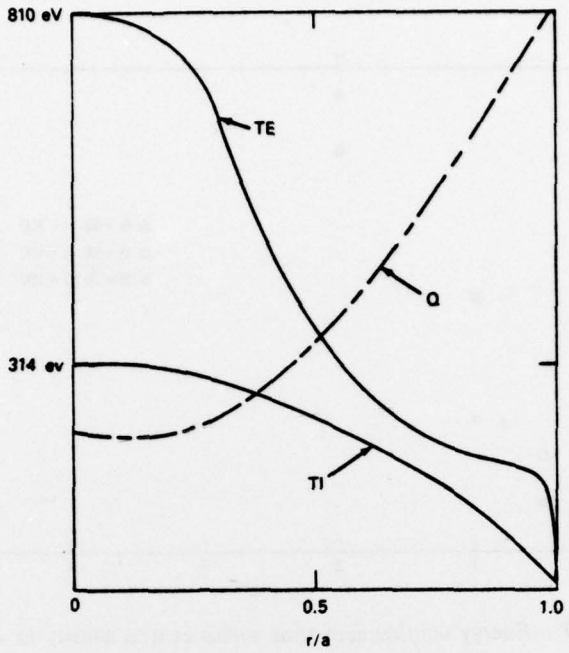

Fig. 11 – Electron and ion temperature profiles in ATC

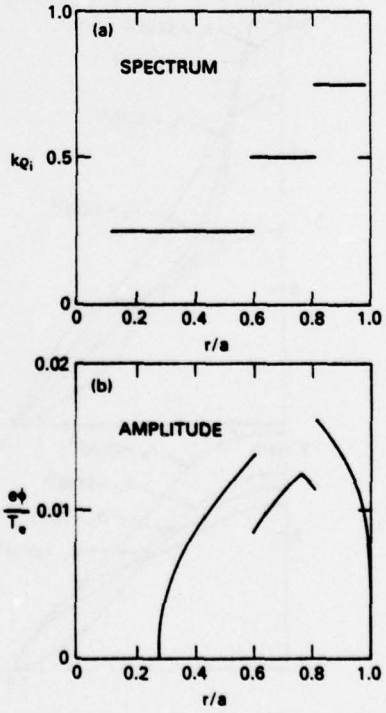

Fig. 12 – (a) The most unstable mode as a function of r/a in ATC and (b) the fluctuation level implied by the numerically determined anomalous transport